Journal of Geology & Geophysics
ISSN: 2381-8719

Research Article
Open Access

Origin of the Arima-type and Associated Spring Waters in the Kinki District, Southwest Japan

Hitomi Nakamura[1,2]*, Kotona Chiba[1], Qing Chang[1], Noritoshi Morikawa[3], Kohei Kazahaya[3] and Hikaru Iwamori[1,2]

[1]*Japan Agency for Marine–Earth Science and Technology, 2-15 Natsushima-cho, Yokosuka-shi, Kanagawa 237-0061, Japan*
[2]*Department of Earth and Planetary Sciences, Tokyo Institute of Technology, 2-12-1 Ookayama, Meguro-ku, Tokyo 152-8551, Japan*
[3]*Geological Survey of Japan, AIST, 1-1-1 Higashi, Tsukuba, Ibaraki 305-8567, Japan*

Abstract

Rare earth elements (REEs) of the spring waters upwelling in the non-volcanic fore-arc region of the Kinki district in southwest Japan were investigated to assess their upwelling processes and deep-seated origins. A principal component analysis of the REE data identified three principal components (PCs) that cover 89% of the entire sample variance: (1) PC-01, which corresponds to a dilution process by which fluids are introduced at low concentrations, previously represented by major solute binary trends, including $\delta^{18}O$–δD systematics; (2) PC-02, which is a precipitation process of REEs from the brine; and (3) PC-03, which is an incorporation of REEs from country rock by carbonic acidity, although the types of country rocks may also have a significant impact on the spring water compositions. Based on these three PCs, together with the major solute concentrations and hydrogen, oxygen, and helium isotopic compositions determined in previous studies, five distinct types of spring waters in the Arima and Kii areas were identified: (i) "Tansansen", (ii) "Kinsen", (iii) "Ordinary Arima", (iv) "Ginsen", and (v) "Eastern Kii". These five types probably represent (ii) a deep brine, (iii) an evolved deep brine that precipitated REE-bearing minerals, (iv) a mixture of (iii) and meteoric water, (v) a meteoric water carbonated by deep gas derived from (ii), and (i) a spring water similar to (v) with a more significant influence of the country rock constituting the aquifer. A comparison of the spring waters in the Arima and Kii areas revealed systematic geographic distributions. The "Ordinary Arima"-type occurs along the Median Tectonic Line, and the "Eastern Kii"-type occurs in the eastern part of the Kii area. The latter seems to upwell in the restricted region where deep low-frequency tremors are observed. We suggest that the geographical distributions are linked to the tectonic setting and/or temporal evolution of fluid upwelling.

Keywords: Brine; Spring water; Subducting slab; Fluid; Arima; Kii

Introduction

Deep-seated geofluids play crucial roles in geological processes at subduction zones, including magmatism, hydrothermal activity, ore formation, and seismicity. For example, reductions in the melting temperatures of rocks by the introduction of slab-derived fluids are thought to be key to understanding arc magmatism with characteristic geochemical signatures, based on experimental and theoretical studies of igneous petrology [1]. However, direct observations and evidence of natural geofluids are rare because of their inaccessibility. The contribution of fluid to seismicity has been studied extensively because fluids may reduce the mechanical strength of rocks and plate boundaries [2]. In southwest and central Japan (Figure 1), deep low-frequency (DLF) tremors have been detected in an arc-parallel 600-km-wide region beneath the fore-arc area from the Shikoku district in the west to the Kinki and Chubu districts, including the Kii Peninsula, in the east, along the subducting Philippine Sea (PHS) slab, at a depth of approximately 30–40 km. This indicates that the tremors may have been caused by fluid generated by dehydration processes from the subducted PHS slab [3]. DLF-type earthquakes have also occurred locally in some locations (Figure 1), such as beneath Osaka Bay, Arima, and northern Kyoto in the Kinki district [4], and these are also thought, based on three-dimensional seismic tomography [5,6] to have been caused by slab-derived fluids. Despite these seismic observations, direct observations of such fluids have been rare, and more information on the physical nature and chemical compositions of these deep-seated geofluids is required.

The Arima-type brine is a candidate for being such a deep-seated geofluid. It may have originated from the subducted PHS slab [7,8] and could have some connection to DLF seismic events [9]. The Arima-type brine is defined as a spring water found in a non-volcanic fore-arc region [10] and is geochemically characterized by a high Cl content of approximately 40,000 ppm, specific $\delta^{18}O$–δD isotopic ratios, and a high $^{3}He/^{4}He$ ratio, comparable to the mantle value [7,11,12], unlike meteoric water or buried sea water [10,13,14]. In addition to these original definitions, the densest brine (the least diluted by meteoric water) in the Arima area shows essentially the same heavy isotopic compositions (Sr–Nd–Pb isotopic ratios) as the slab-derived fluid of the subducting PHS slab [8]. Nakamura et al. [8] have also found a similarity in the REE pattern between the Arima brine and a slab-derived fluid dehydrated at pressure and temperature conditions that correspond to those of the PHS slab beneath the Arima area, based on experimental and theoretical studies [7,15] that support its slab origin. Nakamura et al. [16] have analyzed both the dense and diluted brines of the Arima spring waters for REEs and have demonstrated that there are significant variations in the REE patterns that reflect several important processes during the ascent of deep brine. They identified at least two different patterns and processes that probably represent (a) significant mineral precipitation from the original deep brine and (b) mixing between the brine and the meteoric water, the former of which has not been identified solely from other elemental or isotopic studies.

Within this context, to investigate both the nature of the original deep brine and the geochemical processes that occur during its ascent, we extended our previous research to include more regional data on

***Corresponding author:** Hitomi Nakamura, Japan Agency for Marine–Earth Science and Technology, 2-15 Natsushima-cho, Yokosuka-shi, Kanagawa 237-0061, Japan, Tel: +81468679764; Fax: +81468679625; E-mail: hitomi-nakamura@jamstec.go.jp

Received January 30, 2016; **Accepted** March 01, 2016; **Published** March 07, 2016

Citation: Nakamura H, Chiba K, Chang Q, Morikawa N, Kazahaya K, et al. (2016) Origin of the Arima-type and Associated Spring Waters in the Kinki District, Southwest Japan. J Geol Geophys 5: 240. doi:10.4172/2381-8719.1000240

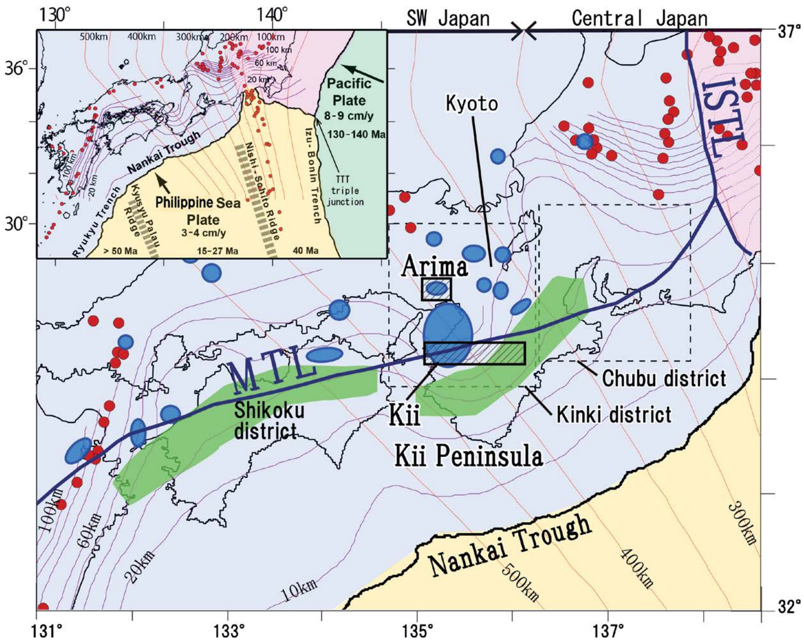

Figure 1: Tectonic setting involved in two continental plates, two oceanic plates, and two large tectonic lines (MTL and ISTL) around Japan as an inset. Enlargement is a map showing the location of the studied areas (Arima and Kii in the shaded square), DLF tremor (green belt) and DLF earthquakes (blue ellipse) based on several studies [3,4,9], the distribution of Quaternary volcanoes (red circles), and the geometry of the subducting Pacific and Philippine Sea slabs relative to the Itoigawa–Shizuoka Tectonic Line (ISTL) and the Median Tectonic Line (MTL). The pink contour lines indicate the depth of the upper surface of the Pacific slab (50 to 300 km depth at 50 km intervals), whereas the purple contour lines indicate that of the Philippine Sea slab (10 to 200 km depth at 10 km intervals). The aseismic parts are indicated by the dotted line.

the Arima-type brine, utilizing both the existing geochemical data from the Arima and Kii areas and new data from the Kii area. In this paper, we first describe the existing data set [7,8,16-18], and we then report new REE data from the Kii area (Figures 1 and 2). We then present the principal component analysis (PCA) results that identify the different sources and processes involved in the deep brine, in contrast to previous studies in which the sources and processes were identified visually. Finally, we discuss the geological and tectonic implications of the results, including the possible connection to basement rock types, fault structures, and seismicity.

Geological and tectonic setting of the studied area

In the Kii Peninsula, spring waters upwell along the Median Tectonic Line (MTL) and subsidiary faults formed in the Miocene (Figures 1 and 2) and exhibit variation in the compositions of the major solute elements and gas phases [7]. These springs appear to upwell through the MTL, dipping northward at approximately 30–40° to 24 km depth, according to seismic reflection profiling in Shikoku [19,20]. The tectonic setting in the southwestern Japan arc is associated with two oceanic plates, the Pacific plate and the PHS, which subduct beneath the studied area from the east at 9 cm/year and from the southeast at 4 cm/year, respectively. The slab surface depth of the Pacific slab is approximately 400 km beneath both the Arima and the Kii areas, whereas that of the PHS is 50–80 km (with considerable uncertainty associated with that estimated range) beneath the Arima area, 30 km beneath the eastern part of the Kii area, and 60 km beneath the western part of the western Kii area (Figure 1) [21,22]. Despite this active subduction, no Quaternary volcanoes have formed in these areas because the Pacific slab is too deep and the PHS is too shallow (Figure 1) to satisfy the physiochemical conditions for melting in the mantle wedge and/or slab [23].

As shown in the geological map of the Kii area (Figure 2), the basement is composed of metamorphic rocks and an accretionary complex associated with metamorphic belts, such as the Sambagawa, Chichibu, and Shimanto Belts, which are bounded by the Mikabu and Butsuzo Tectonic Lines, respectively [24]. The geological structure of the Arima area has been presented elsewhere [16]. The basement rocks are composed of late Cretaceous felsic volcanic rocks such as rhyolite of the Arima Group, granitic rocks including the Rokko granite, and late Eocene to early Oligocene non-marine sedimentary rocks with rhyolitic tuff layers of the Kobe Group [24].

Sample description and analytical method

Existing data set for the arima and kii spring waters

In this study, we utilized the existing data on the spring waters in the Arima area, which is the typical locality of Arima-type brine (Figure 1), and in the Kii area (Figures 1 and 2). We first describe the geochemical characteristics of the existing data from the Arima and Kii areas, and we then describe the sample localities and the analytical method used for the new data from the Kii area. For the Arima area, the data set includes data on the major solutes, $\delta^{18}O$–δD and $^{3}He/^{4}He$ isotopic ratios, Sr–Nd–Pb isotopic ratios, and REE abundances (Table 1) [7,8,16,18]. The Arima spring waters exhibit a wide range of $\delta^{18}O$–δD isotopic ratios and $^{3}He/^{4}He$ isotopic ratios, which are primarily explained by mixing of meteoric water and the deep brine [7,13,14]. The isotopic ratios also exhibit linear variations with major solute elements, such as Cl and Na (Figures 3A-3D), on the basis of which the composition of the deep brine end-member has been estimated [7,14]. The "Kinsen" hot spring is closest to the deep brine end-member, having the highest concentrations of Cl and other solute elements, and the "Tansansen" cold spring is closest to the composition of meteoric water as another end-member, with the lowest solute concentrations

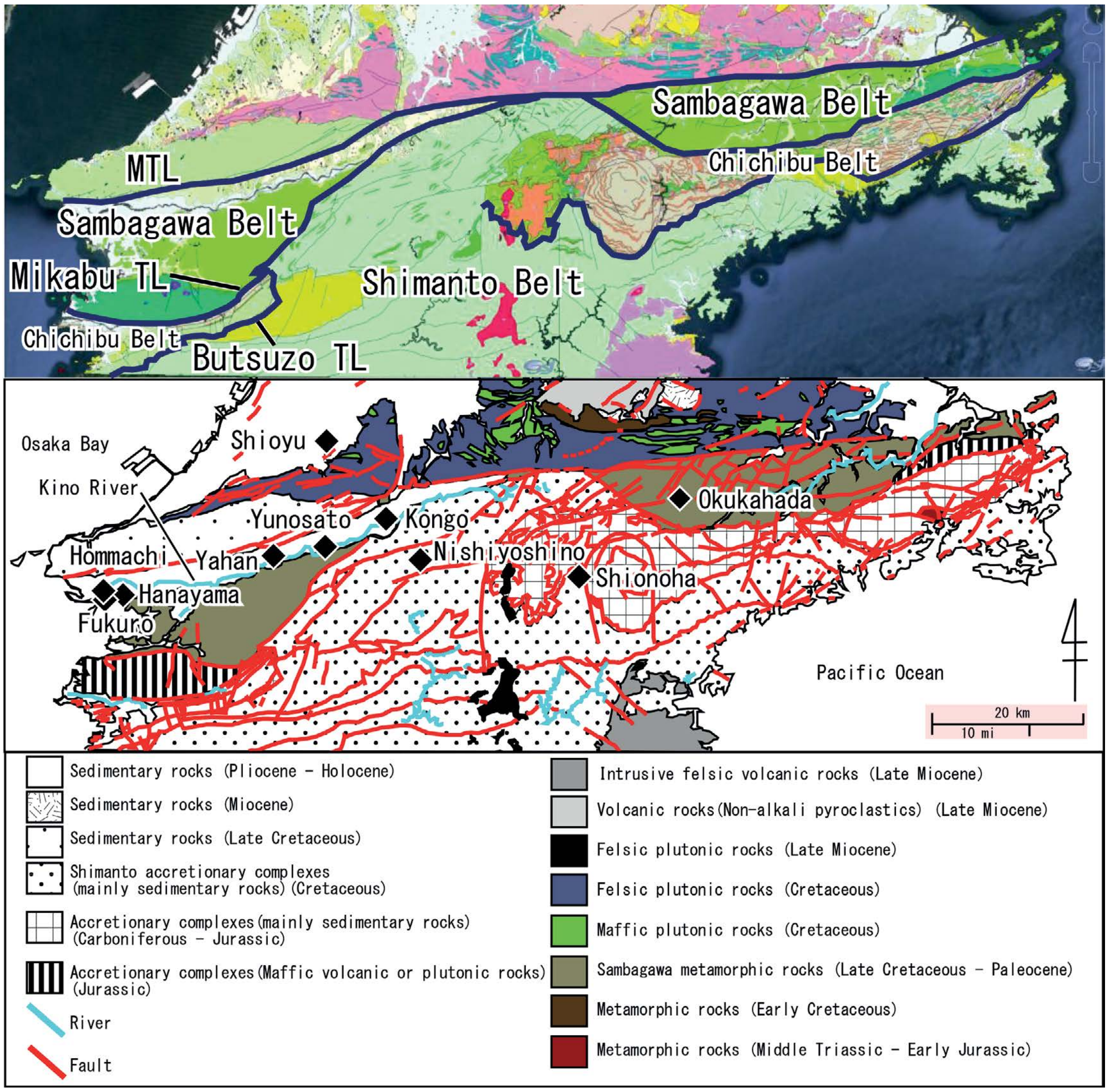

Figure 2: (A) Geologic map of the studied Kii area and three large metamorphic belts (Sambagawa, Chichibu, and Shimanto) exposed in the Kii Peninsula area, modified after Google Earth [35]. The Mikabu and Butsuzo tectonic lines (TL) are roughly aligned along the MTL. (B) Detailed geologic basements, faults, rivers, and locations of the studied spring waters in the Kii area, modified after the seamless digital geological map of Japan [24].

(Figures 3 and 4). Other spring waters with moderate Cl and cation concentrations plot between “Tansansen” and “Kinsen”, as shown in Figures 3 and 4. It should be noted that the gas component, including He, behaves differently from the major solute elements and $\delta^{18}O$–δD isotopic systematics because the gas phase has been released from the deep brine to be regassed to “Tansansen”, resulting in “Tansansen” having the highest $^{3}He/^{4}He$ ratio (close to the mantle value) (Figure 3D) [7].

Although simple mixing between the deep brine and the meteoric water is suggested by the above, recent REE studies have identified processes that cannot be observed from the major solute elements and $\delta^{18}O$–δD isotopic systematics [8,16]. Nakamura et al. [16] found four types in the REE pattern of the Arima spring waters, which may represent (a) mineral precipitation from the original deep brine in relatively deep parts and (b) mixing of the original brine or evolved brine that has undergone precipitation with the meteoric water. They inferred that carbonated spring water could have dissolved REEs from the country rocks, which can be seen in the REE pattern of “Tansansen”. These findings suggest that REEs in the spring water provide invaluable information about the processes that occur during the ascent of deep brine.

For the Kii area, a data set containing data on major solutes and $\delta^{18}O$–δD and $^{3}He/^{4}He$ isotopic ratios is available from previous studies (Table 1) [17,18]. However, the REE abundances have not yet been determined. In the Kii Peninsula, spring waters also exhibit a wide range of $\delta^{18}O$–δD and $^{3}He/^{4}He$ isotopic compositions, which can be explained by a mixing of meteoric water and upwelling of the deep-seated Arima-type brine, particularly along the MTL [9,14]. The $\delta^{18}O$–δD isotopes exhibit linear variations with the major solute elements, such as Cl and Na, although the slopes of the trends seem to be different from those of Arima (Figures 3B and 4A). For example, the slope of the $\delta^{18}O$–δD trend is steeper than that of the Arima spring waters (Figure 3A). The spring water “Honmachi”, which has the highest $\delta^{18}O$–δD isotopic ratio, close to that of deep brine, has the highest contents of Cl

Region	Name of spring water	$\delta^{18}O$ [SMOW]	δD [SMOW]	Cl [mg/L]	HCO_3 [mg/L]	$^3He/^4He$_Ra	Na [mg/L]	Ca [mg/L]	K [mg/L]	Mg [mg/L]
Arima	Ginsen	-7.27	-48.92	435	93	5.44	23	8	4	0
Arima	Gokuraku	2.07	-38.15	25088	26	2.33	11945	2192	2525	15
Arima	Gosho	-4.09	-45.92	8742	473	2.75	4700	627	1000	15
Arima	Gosya	-7.00	-51.05	3392	781	6.41	1743	491	208	35
Arima	Inari-kinsen	3.61	-35.11	36602	-	-	18379	2598	112	511
Arima	Kinsen	4.98	-34.12	40033	1293	4.78	20077	3006	1930	136
Arima	Tansansen	-7.88	-50.27	14	30	7.35	18	23	3	1
Arima	Tenjin	2.22	-37.71	25828	137	-	12189	2356	2593	17
Arima	Uwanari	0.77	-40.50	20786	203	2.38	10127	1845	2153	12
Kii	Fukuro	-	-	-	-	-	-	-	-	-
Kii	Hanayama	-5.75	-48.95	9186.24	3060.93	1.52	1177.06	2598.10	15.07	1953.60
Kii	Hommachi	1.04	-40.95	16089.99	4286.61	2.82	9438.73	763.37	101.32	986.46
Kii	Kongo	-	-	-	-	-	-	-	-	-
Kii	Nishiyoshino	-6.61	-54.12	5004.15	2004.51	1.03	3584.72	203.15	139.24	45.79
Kii	Okukahada	-7.98	-50.02	562.76	1635.34	4.91	551.78	196.67	19.14	77.26
Kii	Shionoha	-9.00	-58.25	775.22	1906.88	6.27	669.27	178.15	75.47	31.42
Kii	Shioyu	-2.73	-44.03	12612.91	3018.68	3.83	7549.10	80.17	87.04	868.94
Kii	Yahan	-2.26	-47.48	13378.30	4586.36	3.47	8487.99	582.46	115.12	599.28
Kii	Yunosato	-5.49	-46.75	6146.48	8097.35	1.79	6284.11	183.72	38.98	194.59

Table 1: Major solute elements and isotopic compositions discussed in this study. The data are from [7,17]. No data are available for "Fukuro" and "Kongo."

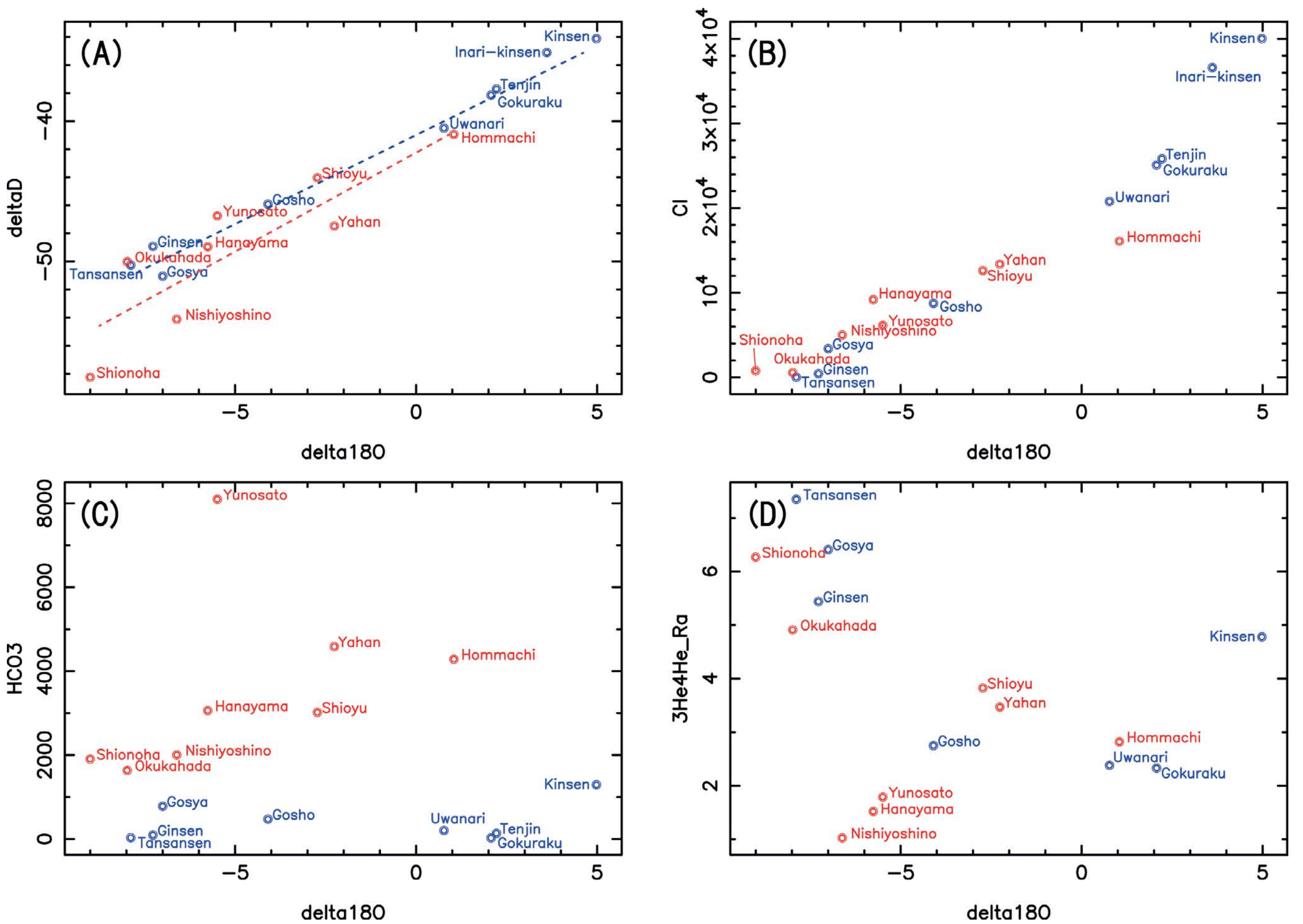

Figure 3: Correlations among $\delta^{18}O$ isotopic ratio versus major solute elements (A) δD isotopic ratio, with a regression line for mixing of meteoric water and a slab-derived fluid as a function of the depth of the subducting slab's steeper slope of the Kii area that corresponds to shallower dehydration than Arima [7,16], (B) Cl abundances (ppm), (C) HCO_3 abundances (ppm), and (D) $^3He/^4He$ isotopic ratios of spring waters, with the names in blue and red for the Arima and Kii areas, respectively. The data were compiled from existing data and are listed in Table 1.

Citation: Nakamura H, Chiba K, Chang Q, Morikawa N, Kazahaya K, et al. (2016) Origin of the Arima-type and Associated Spring Waters in the Kinki District, Southwest Japan. J Geol Geophys 5: 240. doi:10.4172/2381-8719.1000240

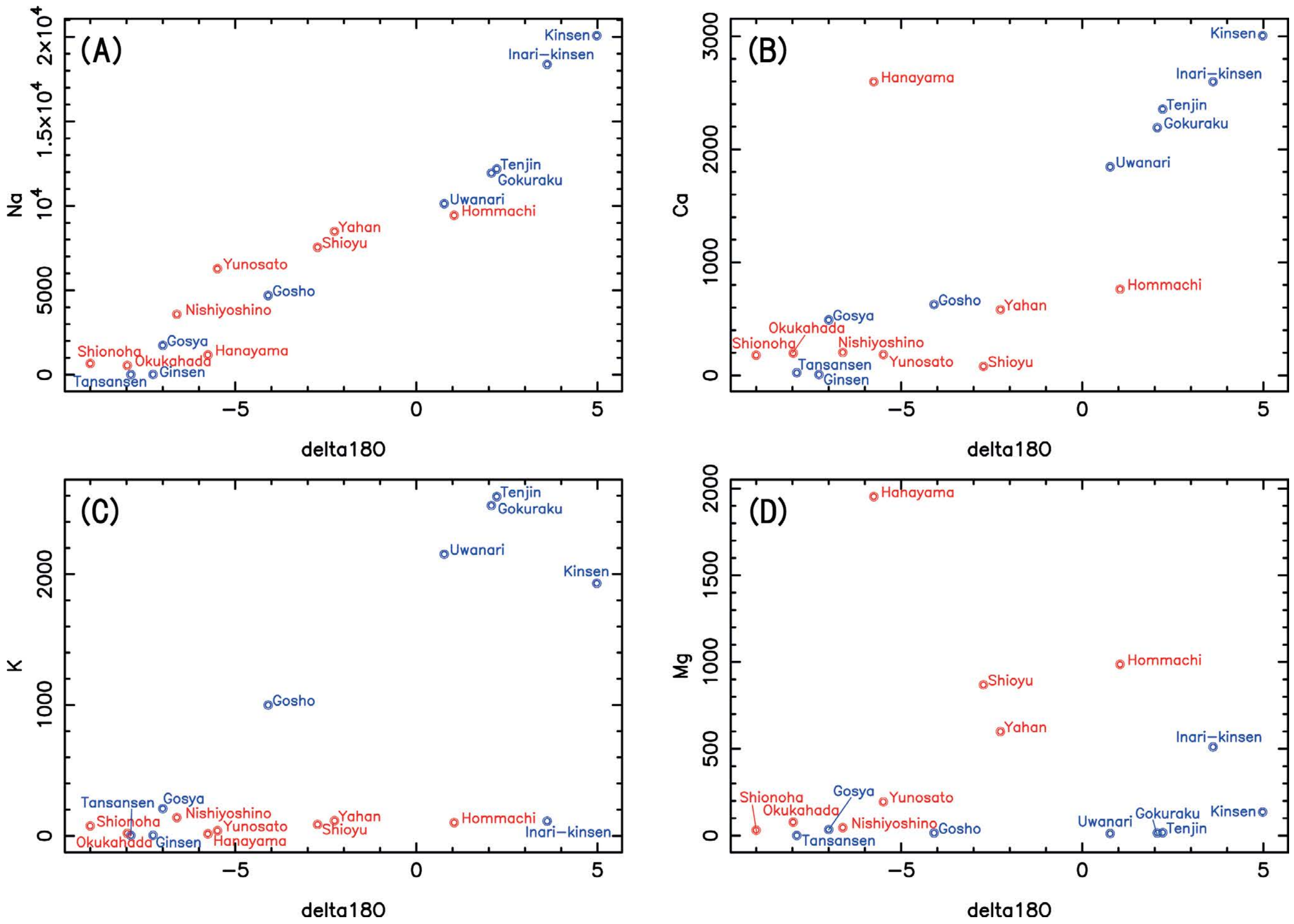

Figure 4: Correlation diagrams between δ^{18}O isotopic ratio versus (A) Na, (B) Ca, (C) K, and (D) Mg in ppm. The color with the name of the type of spring water is the same as in Figure 3.

and other solutes, whereas the spring water "Shionoha", which has the lowest δ^{18}O–δD isotopic ratio, has the lowest concentrations of Cl and lower cations. The concentrations of major solute elements for other spring waters plot between those of the dense "Honmachi" and diluted "Shionoha" waters, except for "Hanayama" (Figures 4B and 4D). Independent behavior of the gas phase, including He, is seen in the Kii area, which is similar to that seen in the Arima area. For example, two spring waters in the Kii area named "Shionoha" and "Okukahada" that have low δ^{18}O–δD isotopic ratios exhibit higher ^{3}He/^{4}He ratios, equivalent to the mantle value [9]. Such variations are similar to those seen for "Tansansen" in the Arima area, which consists of meteoric water with the addition of gas and which may have originated from original deep brine.

Sampling and analytical method for REEs of the Kii spring waters

To supplement the existing data described above, we collected ten spring water samples from the Kii area (Figure 2) for REE analysis. Each sample of 1 to 2 L was collected in a bottle with as much air excluded as possible. No chemicals were added to the samples on site. The analytical method used for the REE analysis of the Kii spring waters followed the method described in Nakamura et al. [16] for the REE analysis of the Arima spring waters. The high salinity and high concentrations of solute elements in the brines interfered significantly with quantitative analysis of the REEs because of the matrix effect. In several cases in which water samples contained visible particles, the particles were dissolved using nitric acid. Considering the matrix effect under high-salinity conditions, we applied the standard addition method for solutions with strong matrix effects [25] and analyzed the samples using inductively coupled plasma mass spectrometry (ICP-MS, iCAP-Qc, ThermoFisher Scientific) at the Japan Agency for Marine–Earth Science and Technology (JAMSTEC). The significant interference from Ba oxides against La, Eu, Nd, Sm, and Gd were quantitatively recalculated after being combined with ^{135}Ba for correction, following the procedure described in Nakamura et al. [16].

Results

The solute major elements and δ^{18}O–δD–He isotopic ratios of the spring waters are summarized in Table 1, and the REE abundances are presented in Table 2 [7,16-18]. The REE compositions are plotted in Figure 5 in spidergram form, normalized with respect to the depleted MORB (mid-ocean ridge basalt) mantle (DMM) [26]. The REE abundances of the Kii and Arima spring waters are approximately three to five orders of magnitude lower than those of the DMM.

Principal component analysis of REE abundances

To examine the processes and/or sources contributing to the generation and upwelling of the spring waters, we performed a principal component analysis (PCA) of the REE abundances of the

spring water	La	Ce	Pr	Nd	Sm	Eu	Gd	Tb	Dy	Ho	Er	Tm	Yb	Lu	Dilution rate
Ginsen	0.2228	0.0093	0.0389	0.2089	0.0773	0.1467	0.0665	0.0161	0.1094	0.0411	0.1799	0.0429	0.3818	0.0769	10.3386
Gokuraku	0.1840	0.0132	0.0216	0.0229	0.1322	10.7723	0.3484	0.0576	0.0214	0.0051	0.0074	0.0474	0.7346	0.1454	1.0000
Gosho	0.0675	0.0013	0.0055	0.0113	0.0339	1.8843	0.0351	0.0061	0.0049	0.0014	0.0033	0.0043	0.0294	0.0099	1.0000
Gosya	0.0946	0.1068	0.0140	0.0557	0.0794	17.0435	0.1776	0.0358	0.1097	0.0700	0.1194	0.1505	0.1398	0.0490	9.9297
Inari-kinsen	0.2901	0.0062	0.0219	0.0115	0.2413	6.8933	0.3182	0.0301	0.0675	0.0184	0.0504	0.0422	0.2696	0.1118	9.6825
Kinsen	3.6382	5.2442	0.5676	2.5409	0.9609	27.8899	1.7651	0.3841	3.6653	0.8360	2.5692	0.3392	2.4161	0.2924	42.2693
Tansansen	4.1881	13.3532	1.9650	10.4090	2.7646	0.3982	4.2497	0.5709	4.1635	0.7909	2.6780	0.3121	2.2442	0.2057	49.9452
Tenjin	1.7895	0.0010	0.0300	0.0126	0.0244	30.1594	0.1479	0.0470	0.0628	0.0118	0.0107	0.0562	0.6806	0.3203	1.0000
Uwanari	0.1236	0.0705	0.0187	0.0599	0.0889	4.4356	0.0928	0.0162	0.0113	0.0038	0.0138	0.0162	0.0889	0.0421	1.0000
Fukuro	0.4664	0.2108	0.0197	0.1407	0.0880	0.9931	0.1371	0.0198	0.3601	0.0815	0.4588	0.1887	0.5590	0.0300	9.6049
Hanayama	0.2820	0.3230	0.0308	0.3936	0.2543	0.5177	0.2981	0.0208	0.3436	0.0640	0.2418	0.0506	0.2409	0.0085	9.5369
Hommachi	0.6209	0.1366	0.0276	0.0355	0.0998	2.4171	0.2168	0.0182	0.0410	0.0114	0.0669	0.0360	0.3804	0.0489	1.0000
Kongo	0.2645	0.0947	0.0208	0.1308	0.0802	0.5578	0.0612	0.0075	0.0310	0.0095	0.0377	0.0268	0.1256	0.0176	1.0000
Nishiyoshino	1.2530	0.0742	0.0041	0.0807	0.0687	6.6262	0.0807	0.1361	0.1887	0.0648	0.2674	0.0617	0.4931	0.0719	9.8453
Okukahada	0.0808	0.1108	0.0157	0.0828	0.0386	0.1289	0.0558	0.0099	0.0635	0.0171	0.0611	0.0111	0.0798	0.0157	9.4315
Shionoha	0.6237	0.4008	0.0578	0.3659	0.0976	1.5612	0.1675	0.0332	0.2384	0.0558	0.1632	0.0218	0.1214	0.0158	1.0000
Shioyu	0.6543	0.3879	0.0292	0.1780	0.1386	2.9333	0.2269	0.0250	0.0393	0.0109	0.0579	0.0407	0.2846	0.0812	9.9690
Yahan	7.1418	1.2716	0.1824	0.6851	0.6683	9.7843	0.3846	0.0968	0.4308	0.0956	0.3013	0.1654	0.3644	0.0528	48.5663
Yunosato	0.1664	0.2148	0.0244	0.1078	0.0258	0.0537	0.0454	0.0057	0.0630	0.0149	0.0542	0.0095	0.0446	0.0045	1.0000

Table 2: Rare earth element (REE) abundances in ppb of spring waters in the Arima and Kii areas.

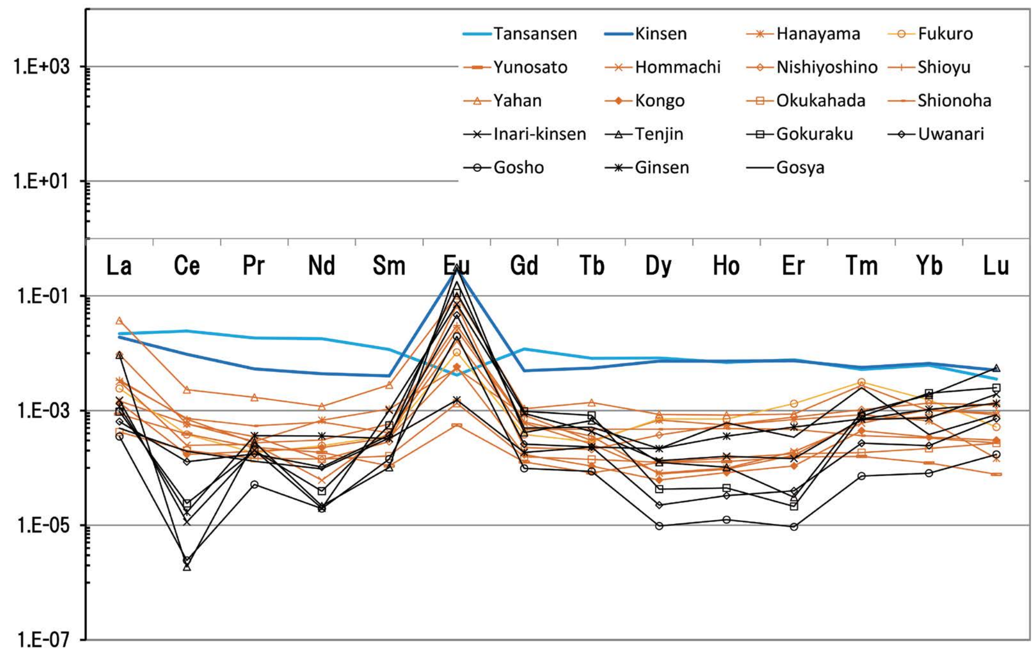

Figure 5: Depleted mid-ocean ridge basalt (MORB) mantle (DMM)-normalized rare earth element (REE) compositions for spring waters, from existing data and newly analyzed samples. The data are listed in Table 2.

spring waters in both the Arima and Kii areas (Table 2). The results show that the most powerful principal component (PC-01), which accounts for 66.8% of the entire sample variance, exhibits a flat REE pattern, as shown in the normalized eigenvector plot (i.e., eigen #1 in Figure 6A). This may indicate that the most dominant process controls the average concentration, moving the REE pattern upward and downward without significantly changing its shape, except for Eu: e.g., dilution by the introduction of fluids with low concentrations having flat REE patterns, such as meteoric water, or dissolution of elements (including REEs with a flat pattern) from source rocks. This possibility was discussed by Nakamura et al. [16], based on visual REE analyses of the Arima spring waters. The second principal component (PC-02) accounts for 17.1% of the entire sample variance and exhibits a strongly convex-downward pattern with a strong positive Eu anomaly (i.e., eigen #2 in Figure 6B). This specific pattern implies differential behaviors among REEs, which provides information that is crucial to deciphering the processes and/or sources involved. Based on geochemical observations of spring waters in the Arima area, Nakamura et al. [16] argued that such a convex-downward pattern may represent a process of precipitation of minerals, such as coprecipitation

Citation: Nakamura H, Chiba K, Chang Q, Morikawa N, Kazahaya K, et al. (2016) Origin of the Arima-type and Associated Spring Waters in the Kinki District, Southwest Japan. J Geol Geophys 5: 240. doi:10.4172/2381-8719.1000240

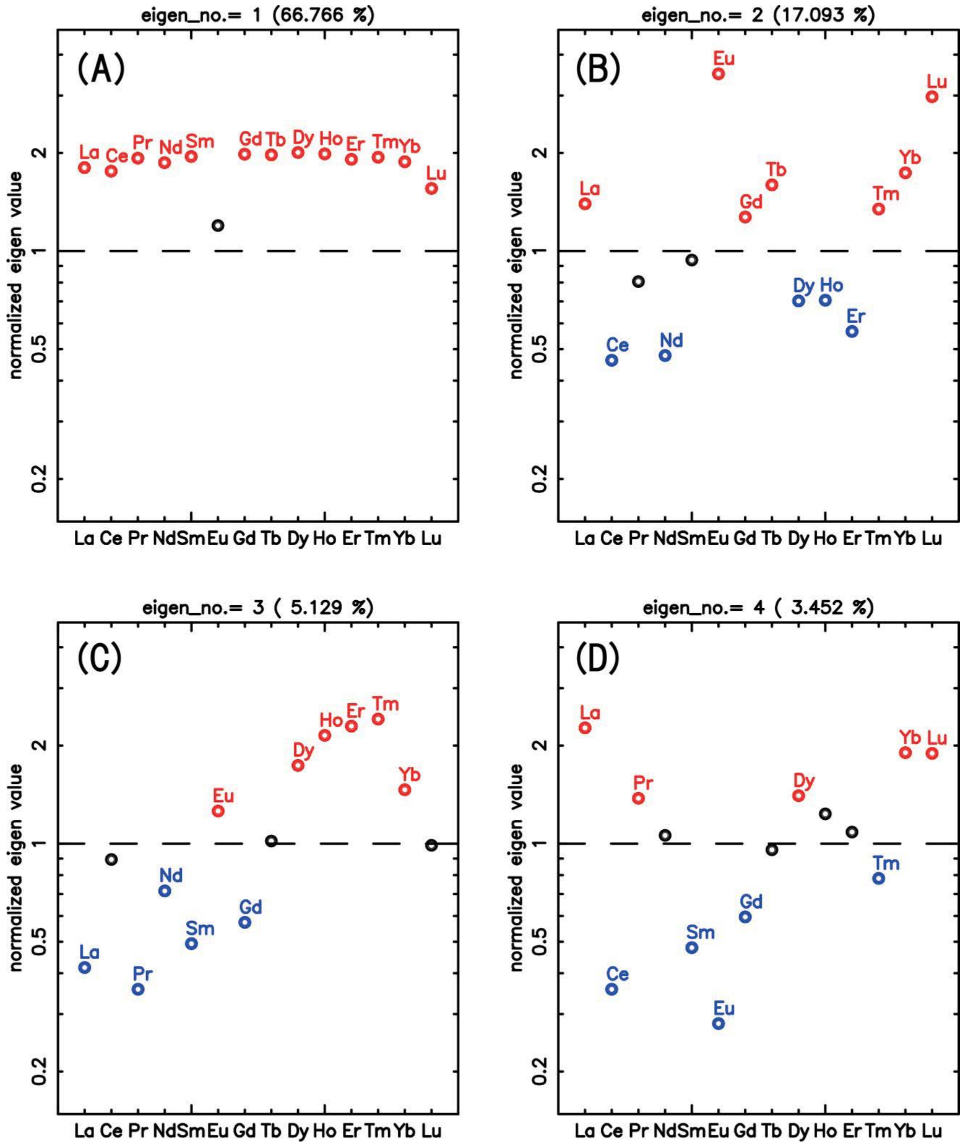

Figure 6: Normalized eigenvector plots. (A) The most powerful principal component (PC-01) accounts for 66.8% of the entire sample variance and exhibits a flat REE pattern (eigen #1). (B) The second principal component (PC-02) accounts for 17.1% exhibits a strongly convex-downward pattern with a strong positive Eu anomaly (eigen #2). (C) The third principal component (PC-03) accounts for 5.1% exhibits an undulation of the overall slope of the REE pattern (eigen #3). (D) The fourth principal component (PC-04) accounts for 3.5% and exhibits a depletion around MREEs, especially those associated with negative Ce anomalies (eigen #4).

of REEs with Fe oxyhydroxides. The third principal component (PC-03) accounts for 5.1% of the entire sample variance and corresponds to a contrasting behavior between light REEs (LREEs) and heavy REEs (HREEs)—in other words, an undulation of the overall slope of the REE pattern, shown as eigen #3 in Figure 6C. The apparent slope of this pattern is positive in Figure 6C, i.e., LREEs < HREEs in terms of eigenvalues. It should be noted that the eigenvectors of the PCs indicate a direction and magnitude of variance measured from the average value of the data and span the compositional space in the directions of both positive and negative signs of the eigenvectors. Therefore, in the case of PC-03, systematic variations in both LREEs < HREEs and LREEs > HREEs are described by PC-03 with opposite signs. The fourth principal component (PC-04) accounts for 3.5% of the entire sample variance and corresponds to a depletion around MREEs, especially those associated with negative Ce anomalies (eigen #4 in Figure 6D). The principal components PC05 to PC13 are less significant in terms of the sample variance, accounting for 3.0, 1.3, 1.1, 0.81, 0.64, 0.35, 0.31, 0.11, 0.032, and 0.018%, respectively. Therefore, a significant portion of the data variation (89.0% of the sample variance) can be explained by the first three PCs (PC-01, 02, and 03). This indicates that several (but not many) processes and/or sources are potentially involved in determining the REE patterns of these spring waters during generation and upwelling in the Arima and Kii areas.

Classification of spring waters based on PCA

As shown in the score plots for individual samples (Figures 7A-7C), we can classify the spring waters based on the scores. Using the powerful first three PCs, we characterize the individual spring waters and the regional differences between the Arima and Kii areas. For the Arima spring waters, there is a wide range in PC-01 from “Gosho” (minimum) to “Tansansen” (maximum), whereas PC-02 exhibits a

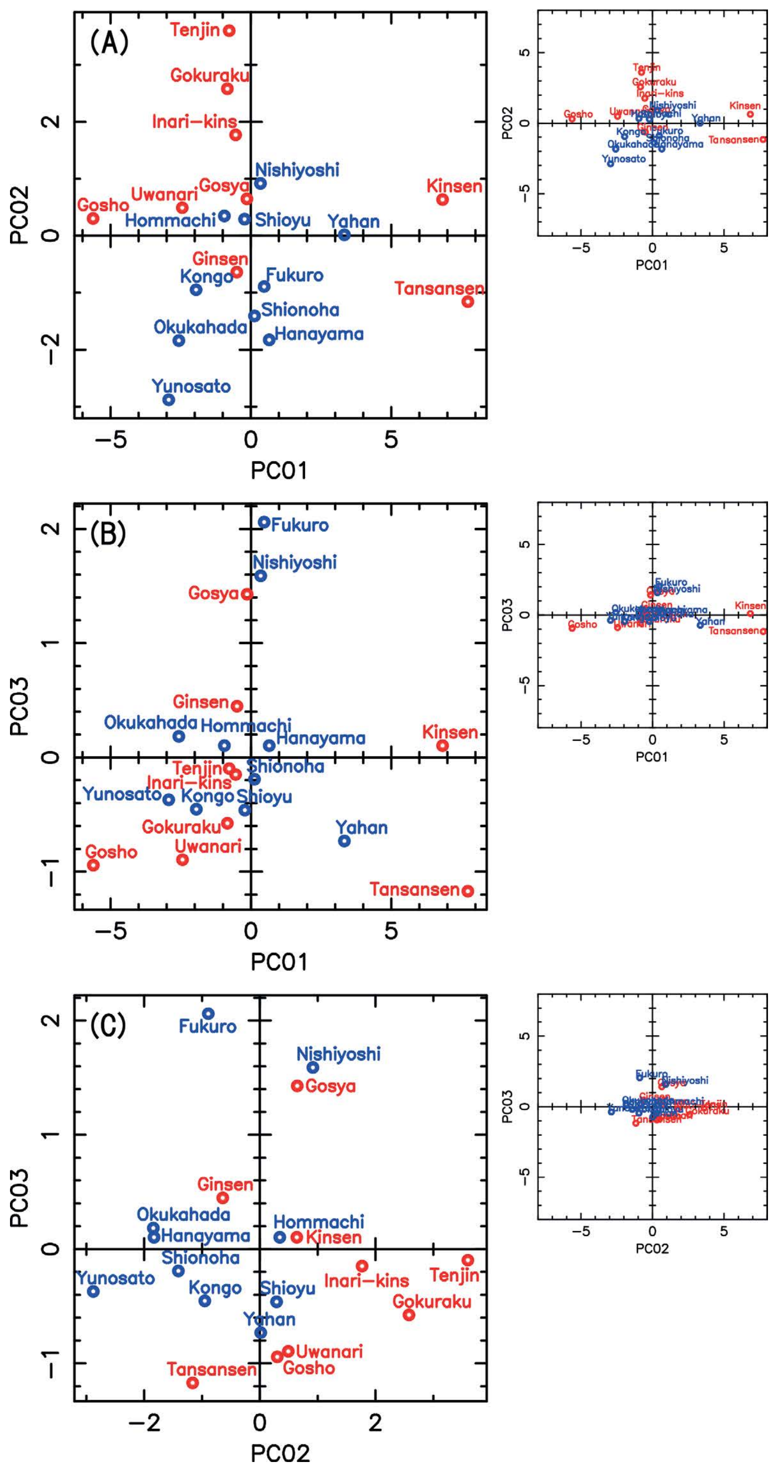

Figure 7: Score plots of individual samples (with names in the same colors as in Figure 3), with spring waters classified based on the scores. Combinations of the powerful three PCs are shown in (A) PC-01 vs. PC-02, (B) PC-01 vs. PC-03, and (C) PC-02 vs. PC-03.

smaller range from "Tenjin" (maximum) to "Ginsen"/"Tansansen" (minimum), as shown in Figure 7A. Two distinct spring waters, "Kinsen" and "Tansansen", between which other spring waters are broadly plotted in terms of their major solute concentrations and $\delta^{18}O$–δD diagrams (Figures 3A-3D and 4A-4D), have high REE abundances, as shown in the spidergram (Figure 5), and exhibit large positive PC-01 scores. Because "Tansansen" plots very close to the meteoric water composition in terms of its major solute concentrations and $\delta^{18}O$–δD, PC-01 and the high REE abundances of "Tansansen" require specific processes and/or sources different from those identified by the conventional measures with the major components, including $\delta^{18}O$–δD, as will be discussed. The PC-03 score exhibits a relatively limited range in the Arima area, from "Tansansen" (minimum) to "Gosya" (maximum).

For the Kii spring waters, there is a smaller range in PC-01 from "Yunosato" (minimum) to "Yahan" (maximum), as shown in Figure 7A. These limits correspond to the highest and lowest REE abundances, respectively (Figure 5). The overall range of PC-02 is smaller than that for the Arima spring waters, with four spring waters ("Hommachi", "Nishiyoshino", "Shioyu", and "Yahan") having positive scores and six spring waters ("Fukuro", "Hanayama", "Kongo", "Okukahada", "Shionoha", and "Yunosato") having negative scores. The large positive PC-02 score commonly observed in the Arima area is not seen in the Kii spring waters. The score variability of the Kii spring waters is smaller than that in the Arima area, which may indicate that the source and/or dilution process involved in the Kii spring waters is relatively uniform, even though the studied area in the Kii is wider than that in the Arima (Figure 1 and 2). Strong positive PC-03 scores were observed for two spring waters ("Nishiyoshino" and "Fukuro") in the Kii area, while a negative score was observed for "Yahan" (Figures 7B and 7C).

Based on these observations, coupled with information on the major solute elements, we can deduce the multi-dimensional compositional variations of the Arima-type brine. The correlations of major solute elements ($\delta^{18}O$, Cl, HCO_3, and $^3He/^4He$ in Ra units, indicating a multiple of the present-day atmospheric value 1.38×10^{-6}) with the individual PC scores (PC-01, PC-02, and PC-03) are shown in Figures 8A-8L, respectively. The plot of PC-01 vs. $\delta^{18}O$ clearly discriminates "Kinsen" from "Tansansen", although both have a high PC-01 score, and five spring waters ("Gokuraku", "Gosho", "Inari-kinsen", "Tenjin", and "Uwanari") are plotted in the area of relatively high $\delta^{18}O$ and negative PC-01 (Figure 8A). The remaining two spring waters of Arima ("Ginsen" and "Gosya") and almost all of the spring waters of the Kii area are plotted in the area of lower $\delta^{18}O$ with a smaller PC-01 score. Therefore, at least four types of spring water can be recognized, which is consistent with the score plot of PC-01 vs. PC-02 (Figure 7A). This classification is also observed in the plots of Cl and HCO_3 (Figures 8B and 8C). However, there is no clear correlation indicated by the plot of PC-01 vs. $^3He/^4He$, indicating that the gas phase behaves independently (Figure 8D). The $\delta^{18}O$ variation exhibits a moderately positive correlation with PC-02 (Figure 8E), with a higher value for the Arima spring waters and a lower one for the Kii spring waters, in contrast to that shown in the PC-01 plot (Figure 8A). This correlation is also observed in the Cl plot (Figure 8F), which is divided into a positive group for the Arima area and a negative group for the Kii area with respect to PC-02 for a similar Cl content. The involvement of PC-02 in a precipitation process at a meteoric aquifer seems to be related to a source for or process of deep brine. The plot of PC-02 vs. HCO_3 (Figure 8G) obviously shows a higher HCO_3 content in the Kii spring waters than in those in the Arima area, which also suggests that the PC-02 score is not linked to the HCO_3 behavior. The $^3He/^4He$ content shows no correlation with PC-02 in either area (Figure 8H). The plot of PC-03 vs. $\delta^{18}O$ illustrates the variation in the spring waters in the Kii area, while a positive correlation from "Tansansen" to "Kinsen" for the five spring waters (with PC-03 < 0) is observed in the Arima area (Figure 8I). The remaining two Arima spring waters, "Ginsen" and "Gosya", are plotted separately, along with the Kii spring waters. A similar variation (in terms of scatter for the Kii spring waters and the positive trend in the Arima area) is also confirmed in the plot of Cl (Figure 8J). Although the solute HCO_3 content exhibits no clear correlation with PC-03, there is a moderate correlation with the $^3He/^4He$ isotopic ratios in the two areas, with two exceptions ("Tansansen" and "Nishiyoshino"). Based on these observations, we can classify the spring waters into several types, possibly induced by three process or origin, that differ from a simple mixing process between the deep brine and meteoric water previously suggested by the major solute and $\delta^{18}O$–δD isotopic systematics [7].

Discussion

Origin and upwelling process of spring waters in Kii

One of the differences between the Arima and Kii areas is that the slope of the Kii spring waters is distinct from that of the Arima spring waters in the $\delta^{18}O$–δD plot (Figure 3A). This difference may be attributed to a difference in the depth of dehydration at the subducting slab: the steeper slope in the Kii area corresponds to shallower dehydration, compared to the Arima area, which has a gentler slope [7,18]. This difference can also be observed in other plots, such as the $\delta^{18}O$–Cl plot in Figure 3B: the slope of the trend is gentler in the Kii area than in the Arima area. These observations suggest that the dense end-member in the Kii area has lower salinity that in the Arima area, possibly reflecting a different chemistry of the slab-derived fluids. On the other hand, the variable trends of major solute cations, such as K and Mg (Figures 4C and 4D), may represent local mechanisms within individual areas of Arima and Kii. The K content is almost constant for the Kii area, whereas it exhibits a large range in the Arima area, and the Mg content increases toward the denser spring water in the Kii area, whereas that in the Arima spring waters is almost constant and at a low level (Figure 4D). These observations could reflect differences in the geology and basement rock types in the two areas, especially those surrounding the meteoric aquifers through which spring waters upwell [16]. In the Arima area, a positive Eu anomaly correlated with the K content is observed, which may be the result of an interaction between hot water and wall rock containing feldspar [27].

We now discuss the origin and upwelling process of spring waters in both areas, especially the Kii spring waters, for which REE data are reported for the first time in this paper. The PCA results show that the PC-01 score is involved in the dilution process. In this regard, PC-01 is expected to have a high correlation with $\delta^{18}O$–δD isotopic ratios, which are robust and commonly used indices for specifying a mixing ratio of meteoric water. As Figure 8A shows, most of the Arima spring waters, including the most primitive deep brine "Kinsen" and five hot spring waters, exhibit a clear positive correlation. However, the cold spring waters "Tansansen", "Ginsen", and "Gosya", as well as most of the Kii spring waters, plot off the Arima trend and exhibit significant scatter. "Tansansen" has the highest PC-01 and lowest $\delta^{18}O$, which is interpreted as being due to the introduction of REEs from the aquifer country rocks into the highly carbonated waters such as "Tansansen" [16]. The same is true for "Ginsen" and "Gosya", but to a lesser extent. The Kii spring waters, most of which are highly carbonated, should have undergone such an effect, which may explain the relatively high REE abundances, represented by moderate PC-01 scores.

The common Arima-type brine, with moderately high $\delta^{18}O$–δD isotopic ratios and moderately high Cl concentrations, exhibit positive PC-02 scores. The spring waters "Honmachi", "Nishiyoshino", "Shioyu", and "Yahan", located along the Kino River, which is associated with the MTL (Figure 2) and five spring waters in the Arima area, can be classified as belonging to this "Ordinary Arima"-type brine. These spring waters have a convex-downward REE pattern detected as eigen #2 (Figure 6B), with a moderately high $\delta^{18}O$–δD signature, indicating that (i) the dilution effect of the deep brine component by meteoric water is limited, which is consistent with the moderate values of PC-01 (Figure 6A), and (ii) the precipitation of REEs, possibly by oxyhydroxides [16], does not affect the $\delta^{18}O$–δD systematics. This

Citation: Nakamura H, Chiba K, Chang Q, Morikawa N, Kazahaya K, et al. (2016) Origin of the Arima-type and Associated Spring Waters in the Kinki District, Southwest Japan. J Geol Geophys 5: 240. doi:10.4172/2381-8719.1000240

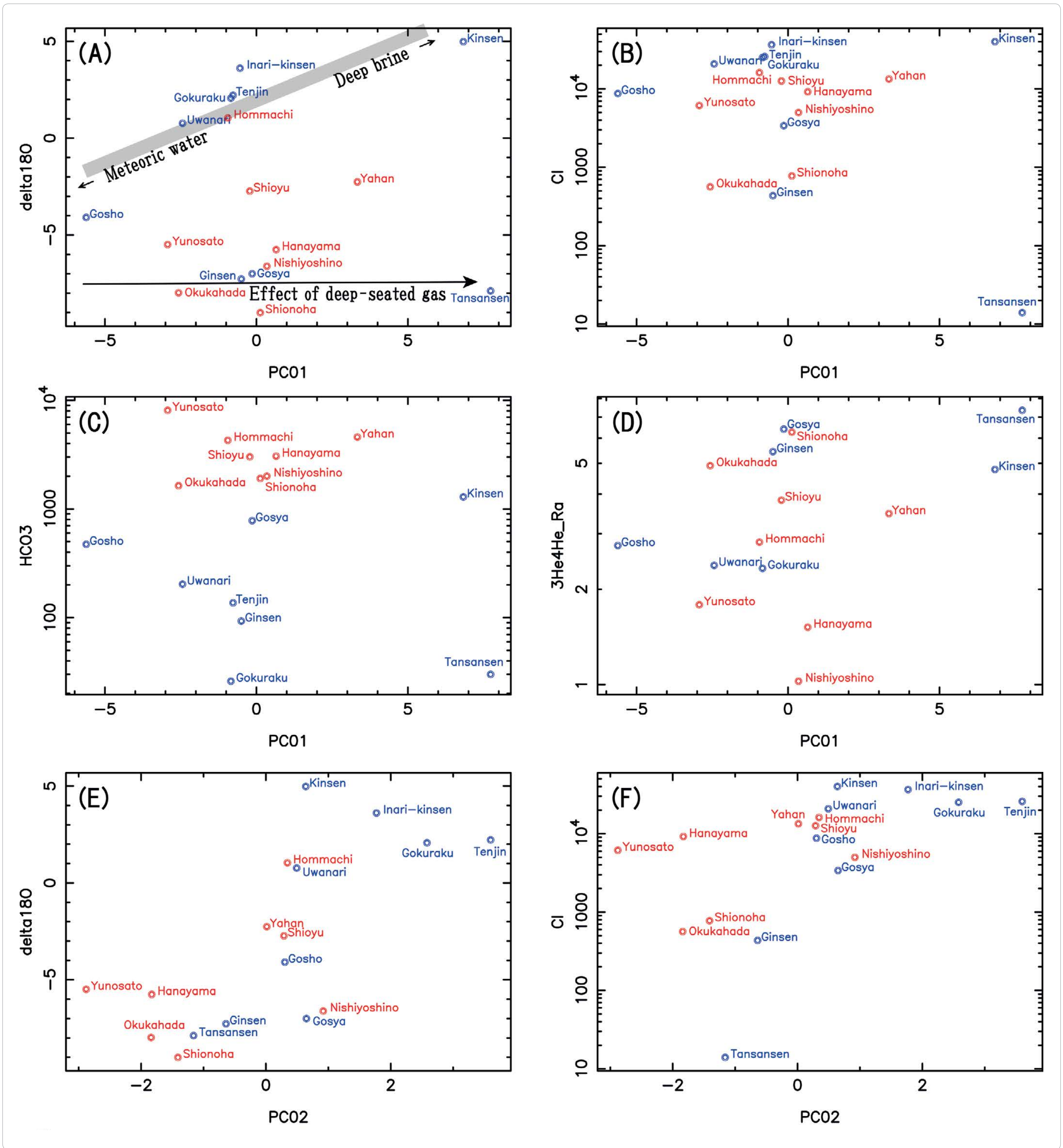

Citation: Nakamura H, Chiba K, Chang Q, Morikawa N, Kazahaya K, et al. (2016) Origin of the Arima-type and Associated Spring Waters in the Kinki District, Southwest Japan. J Geol Geophys 5: 240. doi:10.4172/2381-8719.1000240

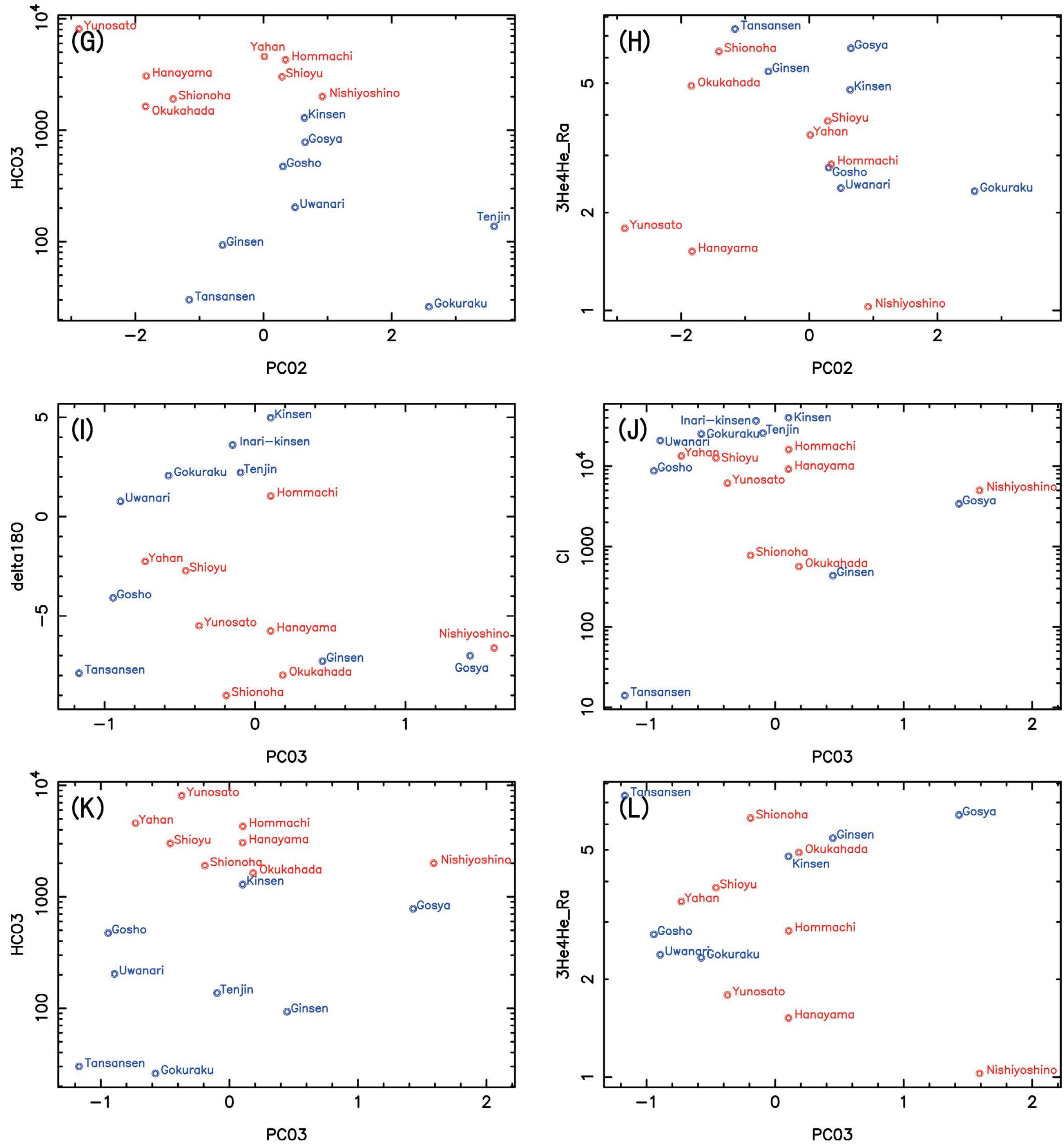

Figure 8: Correlation diagrams for PC-01 vs. (A) ^{18}O, (B) Cl abundances (ppm), (C) HCO_3 abundances (ppm), and (D) $^3He/^4He$ in Ra. (E) ^{18}O, (F) Cl abundances (ppm), (G) HCO_3 abundances (ppm), and (H) $^3He/^4He$ in Ra are plotted against PC-02 on the x axis. (I) ^{18}O, (J) Cl abundances (ppm), (K) HCO_3 abundances (ppm), and (L) $^3He/^4He$ in Ra are plotted against PC-03 on the x axis. The names of the types of spring water are shown in the same colors as in Figure 3.

"Ordinary Arima"-type brine corresponds to the NaCl-type spring water classified by Masuda et al. [14] and Morikawa et al. [17]. The positive correlation between PC-02 and the Cl concentration (Figure 8F) may indicate that the precipitation is enhanced for a denser brine with higher REE contents, (high contribution of slab-derived fluid), such as the Arima hot spring waters. On the other hand, most of the Kii spring waters originate from less dense brines and could have undergone less precipitation.

It is worth noting that regional variation is clearly observed in the PC-02 vs. HCO_3 plot (Figure 8G). This is partly due to the different degrees of variation in PC-02 for the Arima and Kii areas, as mentioned

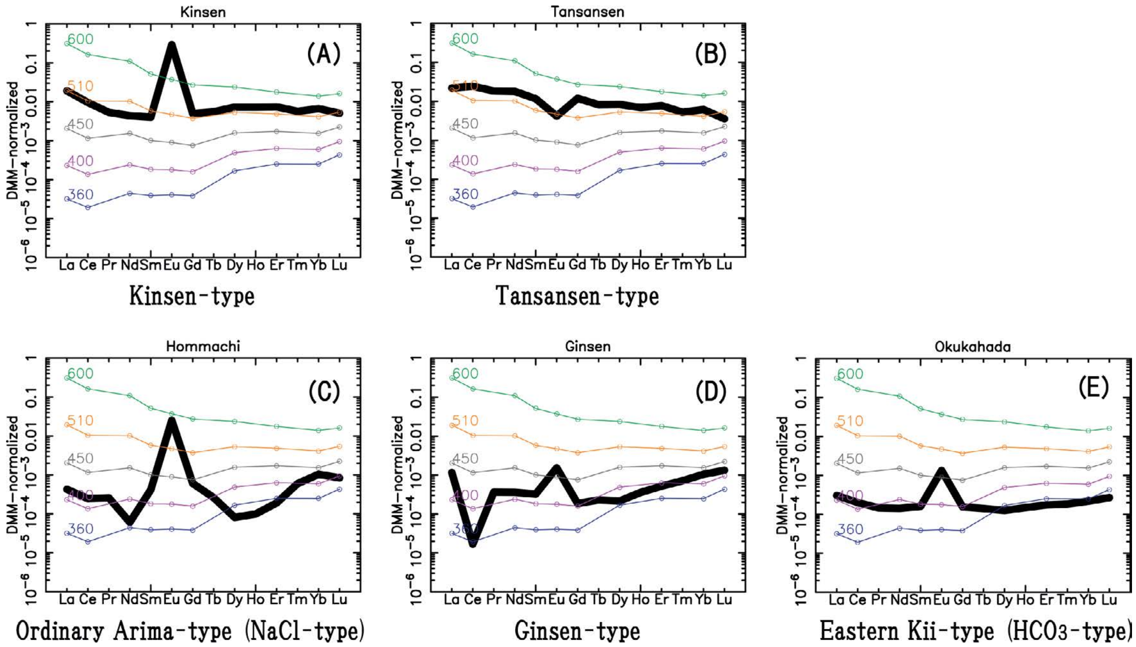

Figure 9: Typical REE patterns shown in spidergram form for (A) "Tansansen"-type, (B) "Kinsen"-type, (C) "Ordinary Arima"-type, (D) "Ginsen"-type, and (E) "Eastern Kii"-type spring waters. The color contours show the composition of fluid derived from altered oceanic crust at 360 to 600° [26-28].

above, but is mostly due to the distinct range in HCO_3. The mechanism that differentiates the areas exhibiting such distinct HCO_3 behavior is unknown at this stage but could be related to the tectonic and geological structure that defines the characteristics of fluid ascent and reactions. For example, fluid ascent through rocks with lower permeability may limit the upwelling velocity which would allow complete separation of the gas component from the deep brine and results in carbonation of the overlying aquifer. The basement rock types in the Kii area are different from those in the Arima area, as will be discussed in section 5.2, and may affect such processes and the amount of REE incorporation that occurs at the aquifer level.

PC-03 is not correlated with either PC-01 or PC-02 (Figures 7B and 7C), which suggests the existence of an independent process involving the origin, partitioning, and source, resulting in an overall contrast between LREEs and HREEs detected as eigen #3 (Figure 6C). This variation may be induced by the presence of gas phases, especially carbonated gas, which enhances the partitioning among host rocks and saline water [16,28,29]. The plot of PC-03 vs. $^3He/^4He$ (Figure 8A) shows a broad positive correlation, which supports the hypothesis of the involvement of gas phases from deep brine, as well as incorporation of significant amounts of REEs from the country rock as a result of the carbonic acid nature of the spring waters [16]. It should be noted that "Tansansen" has a negative PC-03 value but that significant REE incorporation has occurred because of the high carbonic acidity and high $^3He/^4He$ ratio of this water [16]. Because the overall slope of the LREEs/HREEs ratio represented by PC-03 is affected not only by partitioning behavior upon incorporation of REEs but also the REE pattern of the source country rock, in the case of "Tansansen", the involvement of source rock with a high LREEs/HREEs ratio (i.e., a negative PC-03) is suggested, which is consistent with the suggestion that the basement rocks consist of felsic igneous rocks with high LREEs/HREEs ratios [16]. In the Kii area, "Nishiyoshino" has a positive PC-03 score and the lowest He isotopic ratio, which suggests possible contamination of crustal He.

Although the HCO_3 ion content in a water sample may not be directly related to a flux of carbonaceous gas, the HCO_3 abundance in the Kii spring waters exhibits a moderately strong correlation with the $\delta^{18}O$ content that increasing toward the dense end-member (Figure 3C). In the eastern part of the studied area of the Kii Peninsula, two spring waters, "Shionoha" and "Okukahada", are classified as negative PC-02 and moderately positive PC-03, with distinctly high He isotopic ratios (Figures 8H and 8L) and low $\delta^{18}O$–δD isotopic ratios (Figure 3A). These two spring waters referred to as being of the "Eastern Kii" type are similar to "Gosya" in the Arima area, which corresponds to the HCO_3-type classified by Masuda et al. [14] and Morikawa et al. [17]. Morikawa et al. [17] presented the distributions of the Cl concentrations of the spring waters in the Kii Peninsula area and classified them as being Na-Cl-, Na-HCO_3-, Ca-Cl-(or SO_4-), and Ca-HCO_3-dominant types. The distribution of HCO_3-dominant types, including the "Okukahada" and "Shionoha" waters considered in this study, exhibits a moderately positive PC-03 and high He gas, which seems to correspond to the DLF tremor belt detected by seismicity tests [3], whereas the distribution of NaCl-types (that is, "Ordinary Arima"-type brine), distinguished by a positive PC-02, including the "Honmachi", "Nishiyoshino", "Shioyu", and "Yahan" waters considered in this study, are located along the MTL where DLF earthquake activity has been observed (Figure 1). The possible link is discussed in the next section.

Scenarios concerning origin and upwelling of the deep brines and gases

Based on the arguments presented previously, we discuss two scenarios in this section. When the deep brine derived from the PHS slab at a depth of 35–40 km ascends and arrives at a shallow crustal level (a depth of approximately 2000 m), the gas phase formed by decompressional degassing (as suggested by Morikawa et al. [17], based on the gas depth profile) can be separated from the deep brine and ascend to dissolve into meteoric water in the near-surface aquifer system. Such deep gas-bearing water may dissolve REEs from the aquifer country rocks, resulting in a positive PC-03 and a high He gas isotopic ratio, and would be classified as an "Eastern Kii"-type (HCO_3-type) of spring water (Figure 9).

In this case, there are two possible scenarios for the subsequent evolution of the original deep brine that ascended to a depth of approximately 2000 m. One scenario assumes a transient state, i.e., that the original deep brine is still ascending after degassing but has not yet reached the surface. This scenario is consistent with absence of an "Ordinary Arima"-type (NaCl-type) spring in the region where "Eastern Kii"-type (HCO_3-type) springs are dominant (Figures 2 and 9E). It is worth noting that in this "Eastern Kii"-type spring region, DLF tremors and their regional migration over a time scale of days to weeks have been observed (Figure 1), suggesting that deep-seated fluids (possibly deep brine from the slab) could have been repeatedly supplied beneath the region. Such repeated supplies may cause transient upwelling of deep brine that follows the gas phase, which ascends faster than the brine, as a precursor phase of surface effusion of deep brine, although there is no direct evidence of brine ("Ordinary Arima"-type spring) effusion having occurred in the region in the past. If this is the case, an "Ordinary Arima"-type (NaCl-type) spring may occur in the (near) future and coexist with the "Eastern Kii"-type (HCO_3-type) spring, as in the present-day Arima area.

Another steady-state scenario is also possible. In this scenario, the deep brine remains at a depth of approximately 2000 m, where it is degassed and loses some of its buoyancy. In this case, the deep brine ("Ordinary Arima"-type, NaCl-type spring) will never appear on the surface and could disperse. Unlike the "Ordinary Arima"-type (NaCl-type) spring region along the MTL, where many spray faults are present, the fault system is relatively undeveloped in the "Eastern Kii"-type (HCO_3-type) spring region (Figure 1). Accordingly, the fluid pathways along which the deep brine is guided to ascend to the surface are poorly developed, which could be one reason for the absence of "Ordinary Arima"-type (NaCl-type) springs in the eastern Kii area along with the HCO_3-type spring. Slab-derived fluids will exhibit variable REE abundances depending on the temperature of dehydration. With slab dehydration occurring at lower temperatures beneath the fore-arc Kii region (Figure 1), REEs in the slab-derived fluids will exhibit significantly lower abundances because of the strong temperature dependence of the partition coefficient between fluid and residual solids (Figures 9A-9E for slab fluids derived from altered oceanic crust at 360 to 600 degrees) [30,31]. Although the rare occurrence of the original deep brine (i.e., a brine that has not undergone REE-bearing deposition of minerals) prevents us from estimating the physical conditions for slab dehydration accurately, the overall REE level, especially the Lu and La contents, of the "Ordinary Arima"-type (NaCl-type) spring waters in the Kii area is thought to originate from slab-derived fluids generated by dehydration of the slab at approximately 450°C (Figure 9C).

In any case, the original deep brine precipitates REE-bearing minerals to produce spring water variations represented by PC-02 (Figure 7A). As shown in previous studies of the Arima area [16], when the deep brine enters a meteoric aquifer, the precipitation process is likely to be triggered by a change in temperature and oxygen fugacity conditions, simultaneously generating a gas phase that will ascend separately and be added to the shallower aquifer. Within the shallow aquifer, HCO_3-type spring water is produced, enhancing reactions with the basement rocks because of its carbonic acidity. In the Arima area, the basement granite is continuously metasomatized by the intrusion of deeply originated hot water, which makes granite turn to decomposed granite called "Masado" and also enriches the river water with REE [32]. Positive Eu anomalies are commonly observed for both the "Ordinary Arima"-type (NaCl-type) and "Ginsen"-type (HCO_3-type) spring waters in the Arima area, except Tansansen, although the basement granite exhibits a clear negative Eu anomaly [33-35]. When the deep brine encounters near-surface water under oxidizing conditions in the aquifer, the overlapping effects associated with elution of Eu^{2+} from plagioclase of the granite and deposition of other REEs with oxyhydroxides will enhance the strong positive Eu anomaly with a low abundance of Ln^{3+}, as observed in the spidergrams (Figures 5 and 9). This suggests that the basement rock composition and oxidation conditions may have strong influences on the spring water composition. The variability in terms of major solute elements and REEs in the Kii area, illustrated in Figures 3 and 4, could be partly attributed to such an effect, although quantitative modeling to confirm this remains to be performed.

Conclusions

To characterize the Arima-type brine and associated spring waters in the Kii area, we performed REE analyses of the spring waters in a wide area of the Kii Peninsula. In addition, we compiled data on the major solute elements, REE abundances, and $\delta^{18}O$–δD, He, and Sr–Nd–Pb isotopic systematics from previous studies encompassing a broad region of the Arima and Kii areas in southwestern Japan. Based on this data set, we classified the spring waters into several types described below.

The results of a principal component analysis (PCA) of the existing and new REE data from the Kii and Arima areas showed that three principal components (PCs) explain 89% of the entire sample variance. Comparisons between the major solute components (including $\delta^{18}O$–δD isotopic ratios) and the REE systematics represented by these three PCs allow us to categorize the spring waters into the following five types:

(i) "Tansansen" -type: A flat pattern with a negative Eu anomaly, large positive PC-01, large negative PC-02 (Figure 7A), and negative PC-03, observed uniquely as "Tansansen" (Figure 9A) in the Arima area. This spring water exhibits affinities with the HCO_3-type described below but is distinct because of the significant impact of basement granitic rocks.

(ii) "Kinsen" -type: An overall slightly convex-downward REE-pattern with a moderately positive Eu anomaly and large positive PC-01 and PC-02 scores (Figure 7A) and a small positive PC-03, observed uniquely as "Kinsen" (Figure 9B) in the Arima area. This spring water exhibits geochemical features closest to those of the original deep brine from the subducted Philippine Sea slab.

(iii) "Ordinary Arima" -type: A strongly convex-ward pattern with a strong positive Eu anomaly, moderately negative PC-01, positive PC-02, and negative PC-03 (Figures 7A and 8I) and exhibiting the PC-01–$\delta^{18}O$ trend shown in Figure 8A. This type of spring water is derived from type (ii) original brine that has undergone REE-precipitation and is commonly observed in the Arima area, as well as in the Kii area (Figure 9C), although in the Kii area, this type of spring water seem to have some influence from (iv) below that obscures the PC-01–$\delta^{18}O$ trend. This spring water has been classified as being of the NaCl-type (Figure 9C).

(iv) "Ginsen" -type: A slightly convex-downward pattern with a moderately positive Eu-anomaly, moderately negative PC-01, moderately negative PC-02, and positive PC-03 (Figures 7A and 8I), departing from the PC-01–$\delta^{18}O$ trend of type (iii) toward a positive PC-01 due to the gas phase effect (Figures 8A and 8D). This spring water has affinities with both the NaCl-type (deep brine signature) and HCO_3-type (gas-added meteoric water signature), represented as "Ginsen" (Figure 9D), although it is rather diluted.

(v) "Eastern Kii" -type: An almost flat pattern with a moderately positive Eu anomaly, both positive and negative PC-01, negatives PC-02, a moderately negative PC-03, and a high $^3He/^4He$ isotopic ratio (Figures 7A and 8L). These features are similar to those of type (iv) (the "Ginsen" type), except that type (v) and all other Kii spring waters exhibit high HCO_3 contents (Figures 8C, 8G, and 8K) unlike type (iv) and all other Arima spring waters. These types of spring waters, which occur only in the eastern part of the studied Kii area, are represented by "Okukahada" and "Shionoha" and have been conventionally classified as belonging to the HCO_3-type (Figures 9E).

It should be noted that the five types (i) to (v) described above are accounted for by a combination of a smaller number of processes and sources: (1) mixing between the slab-derived deep brine and meteoric water (represented by major solute binary trends, including $\delta^{18}O$–δD systematics, as well as a part of PC-01), (2) precipitation of REEs from the brine (represented by PC-02), and (3) incorporation of REEs from the country rock by carbonic acidity (represented by PC-03), although the type of country rocks (i.e., granitic rocks, metamorphic rocks) may also have a significant impact on the spring water composition. In addition, the compositional variability of slab-derived fluid with temperature and depth of slab dehydration probably influences the regional differences observed between the Arima and Kii areas. In comparing the spring waters in the Arima and Kii areas, we detected systematic geographic distributions of the NaCl-type and HCO_3-type waters in the Kii area. The former upwells along the MTL, whereas the latter upwells in the eastern part of the studied area, where DLF tremors have been observed. This suggests that the geographic distributions are linked to the tectonic setting and/or temporal evolution of upwelling of the slab-derived fluid.

Acknowledgments

This work was supported by JSPS KAKENHI Grant Number 25400524 and the Earthquake Research Institute Cooperative Research Program of the University of Tokyo.

References

1. Tatsumi Y, Eggins S (1995) Subduction zone magmatism. Blackwell, Oxford.
2. Nakajima J, Tsuji Y, Hasegawa A (2009) Seismic evidence for thermally-controlled dehydration reaction in subducting oceanic crust. Geophys Res Lett 36, L03303, doi:10.1029/2008GL036865.
3. Obara K (2002) Nonvolcanic deep tremor associated with subduction in southwest Japan. Science 296: 1679-1681.
4. Takahashi H, Miyamura J (2009) Deep low-frequency earthquakes occurring in Japanese islands. Geophysical Bulletin of Hokkaido University 72: 177-190.
5. Zhao D, Kanamori H, Negishi H, Wiens D (1996) Tomography of the source area of the 1995 Kobe earthquake: Evidence for fluids at the hypocenter? Science 274: 1891-1894.
6. Zhao D, Tani H, Mishra OP (2004) Crustal heterogeneity in the 200 Tottori earthquake regions: Effect of fluids from slab dehydration. Phys Earth Planet Inter 145: 161-177.
7. Kusuda C, Iwamori H, Nakamura H, Kazahaya K, Morikawa N (2014) Arima hot spring waters as a deep-seated brine from subducting slab. Earth Planets Space 66(1):119. doi: 10.1186/1880-5981-66-119.
8. Nakamura H, Fujita Y, Nakai S, Yokoyama T, Iwamori H (2014) Rare earth elements and Sr–Nd–Pb isotopic analyses of the Arima hot spring waters, Southwest Japan: implications for origin of the Arima-type brine. J Geol Geosci 3:161. doi: 10.4172/2329-6755.1000161.
9. Kazahaya K, Takahashi M, Yasuhara M, Nishio Y, Inamura A, et al. (2014) Spatial distribution and features of slab-related deep-seated fluid in SW Japan. Journal of Japanese Association of Hydrological Science 44: 3-16.
10. Matsubaya O, Sakai H, Kusachi I, Satake H (1973) Hydrogen and oxygen isotopic ratios and major element chemistry of Japanese thermal water systems. Geochem J 7: 123-151.
11. Nagao K, Takaoka N, Matsubaya O (1981) Rare gas isotopic compositions in natural gases in Japan. Earth Planet Sci Lett 53: 175-188.
12. Sano Y, Wakita H (1985) Geographical distribution of 3He/4He ratios in Japan – implications for arc tectonics and incipient magmatism. J Geophys Res 90: 8729-8741.
13. Tanaka K, Koizumi M, Seki R, Ikeda N (1984) Geochemical study of Arima hot-spring waters, Hyogo, 408 Japan, by means of tritium and deuterium. Geochem J 18: 173-180.
14. Masuda H, Sakai H, Chiba H, Tasurumaki M (1985) Geochemical characteristics of Na-Ca-Cl-HCO3 type waters in Arima and its vicinity in the western Kinki district, Japan. Geochem J 19: 149-162.
15. Ayers J (1998) Trace element modeling of aqueous fluid–peridotite interaction in the mantle wedge of subduction zones. Contrib Mineral Petrol 132: 390-404.
16. Nakamura H, Chiba K, Chang Q, Nakai S, Kazahaya K, et al. (2015) Rare earth elements of the Arima spring waters, Southwest Japan: implications for fluid–crust interaction during ascent of deep brine. J Geol Geosci 4:217. doi:10.4172/jgg.1000217.
17. Morikawa N, Kazahaya K, Takahashi M, Inamura A, Yasuhara M, et al. (accepted) Widespread distribution of ascending fluids transporting mantle helium in the fore-arc region and their upwelling processes: Noble gas and major element composition of deep groundwaters in the Kii Peninsula, southwest Japan.
18. Takahashi M, Kazahaya K, Yasuhara M, Tsukamoto H, Sato T, et al. (2011) A database of deep groundwater chemistry. Geol Surv Japan, AIST 532.
19. Ito T, Kojima Y, Kodaira S, Sato H, Kaneda Y, et al. (2009) Crustal structure of southwest Japan, revealed by the integrated seismic experiment Southwest Japan 2002. Tectonophys 472: 124-134.
20. Kawamura T, Onishi M, Kurashimo E, Ikawa T, Ito T (2003) Deep seismic reflection experiment using a dense receive and sparse shot technique for the deep structure of the Median Tectonic Line (MTL) in east Shikoku, Japan. Earth Planets Space 55: 549-557.
21. Nakajima J, Hasegawa A (2007) Subduction of the Philippine Sea plate beneath southwestern Japan: Slab geometry and its relationship to arc magmatism. J Geophys Res 112, B08306, doi:10.1029/2006JB004770.
22. Hirose F, Nakajima J, Hasegawa A (2008) Three-dimensional seismic velocity structure and configuration of the Philippine Sea slab in southwestern Japan estimated by double-difference tomography. J Geophys Res 113, B09315, doi:10.1029/2007JB005274.
23. Iwamori H (2007) Transportation of H_2O beneath the Japan arcs and its implications for global water circulation. Chem Geol 239: 182-198.
24. Geological Survey of Japan, AIST (2015) Seamless digital geological map of Japan 1: 200,000. Geological Survey of Japan, National Institute of Advanced Industrial Science and Technology.
25. Uemoto M (2008) Principles and practices of ICP emission and ICP mass spectrometry, Ohmsha, ISBN 978-4-274-20539-2, Tokyo (in Japanese).
26. Workman RK, Hart SR (2005) Major and trace element composition of the depleted MORB mantle (DMM). Earth Planet Sci Lett 231: 53-72.
27. Teranishi K, Isomura K, Yano M, Chayama K, Fujiwara S, et al. (2003) Measurement of distribution of rare earth elements in Arima-type springs using preconcentration with chelating resin/ICP-MS. Bunseki Kagaku 52: 289-296.
28. Ohta A, Kawabe I (2000) Rare earth element partitioning between Fe oxyhydroxide precipitates and aqueous NaCl solutions doped with NaHCO: Determinations of rare earth element complexation constants with carbonate ions. Geochem J 34: 439-454.
29. Ohta A, Kawabe I (2000) Theoretical study of tetrad effects observed in REE distribution coefficients between marine Fe-Mn deposit and deep seawater, and in REE(III)-carbonate complexation constants. Geochem J 34: 455-473.
30. Spandler C, Hermann A, Arculus R, Mavrogenes J (2003) Redistribution of trace elements during prograde metamorphism from lawsonite blueschist to

eclogite facies; implications for deep subduction-zone processes. Contrib Mineral Petrol 146: 205-222.

31. Kessel R, Schmidt MW, Ulmer P, Pettke T (2005) Trace element signature of subduction-zone fluids, melts and supercritical liquids at 120–180 km depth. Nature 437: 724-727.
32. Nakajima T, Terakado Y (2003) Rare earth elements in stream waters from the Rokko granite area, Japan: Effect of weathering degree of watershed rocks. Geochem J 37: 181-198.
33. Ishihara S, Chappell BW (2007) Chemical compositions of the late Cretaceous Ryoke granitoids of the Chubu District, central Japan-Revisited. Bull Geol Surv Japan 58: 323-350.
34. Terakado T, Fujitani T (1995) Significance of iron and cobalt partitioning between plagioclase and biotite for problems concerning the Eu^{2+}/Eu^{3+} ratio, europium anomaly, and magnetite-/ilmenite-series designation for granitic rocks from the inner zone of southwestern Japan. Geochim Cosmochim Acta 59: 2689-2699.
35. Google Earth (2013) accessed April 10, 2013.